Superoxide anions disproportionation induced by Li^+ and H^+: pathways to $^1O_2$ release in Li-O_2 batteries

Adriano Pierini,[a] Sergio Brutti,[a] and Enrico Bodo*[a]

[a] Dr. Adriano Pierini, Prof. Sergio Brutti, Prof. Enrico Bodo
Dipartimento di Chimica
Università di Roma La Sapienza
P.le Aldo Moro 5, 00185 Roma (Italy)
E-mail: enrico.bodo@uniroma1.it

Abstract: We explore the disproportionation reaction of superoxide anions in the presence of H^+ and Li^+ cations with high quality multiconfigurational ab-initio methods. This reaction is of paramount importance in Li-O_2 battery chemistry as it represents the source of a major degrading impurity, singlet molecular oxygen. For the first time, the thermodynamic and kinetic data of the reaction are drawn from an accurate theoretical model where the electronic structure of the reactant and products is treated at the necessary level of theory. Overall, the H^+ catalyzed O_2^-+O_2^- disproportionation follows a very efficient thermodynamic and kinetic reaction path leading to neutral $^3O_2$, $^1O_2$ and peroxide anions. On the contrary, we have found that the Li^+ catalysis promotes only the release of $^3O_2$ whereas the $^1O_2$ formation is energetically unfeasible at room temperature.

Introduction

The aprotic lithium-oxygen battery technology (aLOB) is both a fundamental and technological challenge. [1–4] While aLOBs theoretical performance overcomes all other proposed battery chemistries, [5,6] their implementation in real devices requires to successfully tackle many unsolved issues, such as the reversibility of the redox reaction, [7] the parasitic release of CO_2/CO/H_2,[8] the degradation of the electrolyte to Li_2CO_3 or other organic by-products [9–11] and the stability of the lithium negative electrodes[12].

The chemical disproportionation of lithium superoxide R1 is a key step in the complex redox chemistry occurring in aLOBs: [13,14]

$$2LiO_2 \rightleftharpoons Li_2O_2 + O_2 \qquad \text{(R1)}$$

In aLOBs, LiO_2 is a radical intermediate product in the electrochemical reduction of O_2 (i.e. ORR, oxygen reduction reaction, R2) and in the electrochemical oxidation of Li_2O_2 (OER, oxygen evolution reaction, R3) [1,15].

$$O_2 \xrightarrow{+e^-+Li^+} LiO_2 \xrightarrow{+e^-+Li^+} Li_2O_2 \qquad \text{(R2)}$$

$$Li_2O_2 \xrightarrow{-e^--Li^+} LiO_2 \xrightarrow{-e^--Li^+} O_2 \qquad \text{(R3)}$$

Despite its stoichiometric simplicity, R1 hides a complex mechanism landscape that involves singlet-triplet spin intersystem crossing while evolving from two doublet LiO_2 radicals. [16,17] In fact, besides lithium peroxide, the disproportionation product can be either $^1O_2$ or $^3O_2$. [18,19]

Experimentally, the chemical reaction of KO_2 with LiTFSI, that mimics the LiO_2 disproportionation, evolves toward $^3O_2$ and minor quantities of $^1O_2$. [20] This is in line with the expected thermodynamics of the process, being $^3O_2$ the ground state electronic state of the molecular oxygen molecule. The addition of protons or weak Lewis acidic cations increases remarkably the singlet oxygen release. [20]

The appearance of singlet molecular oxygen has been detected in aLOBs, both in electrochemical ORR and OER. [18] The formation of this highly reactive biradical molecule has been attributed to the LiO_2 disproportionation (R1) during ORR, i.e. aLOB discharge, [20] and to the Li_2O_2 oxidation above 3.6-3.8 V vs Li, i.e. aLOB charge. [18,19] Due to the remarkable reactivity of the $^1O_2$ molecule, this chemical species is at the origin of parasitic degradation reactions during electrochemical charge/discharge cycles. [19] Overall, $^1O_2$ paves the way to aLOBs death upon cycling.

Focusing on the superoxide disproportionation, the Wigner-Witmer spin correlation rules (WWSCRs) indicate that doublet-doublet reactions should proceed via the singlet potential energy surface [21] (PES). But, being $^3O_2$ the most abundant product of R1, the reaction mechanism either violates the WWSCRs or occurs though a facile spin intersystem crossing. WWSCRs are strictly valid only for reactions involving diatomic or polyatomic molecules with weak spin-orbit coupling. [22] Having the superoxide radical a spin-orbit coupling constant of ~160 cm^{-1}, [23] an accurate electronic structure analysis of the reaction is mandatory to describe correctly the energetic landscape of R1, both on the singlet and triplet PES's

Here we present a computational model of the bimolecular disproportionation reaction of superoxide anions coordinated by either Li^+ or H^+, to mimic *in silico* one key-reaction step of aLOB ORR and OER mechanisms. We use the Complete Active Space Multiconfigurational Self Consistent Field method (CASSCF) followed by a perturbation treatment of the correlation energy (NEVPT2). The need for a multiconfigurational approach emerges because singlet oxygen (and possibly the entire reactive path that leads to its formation) has a strong multideterminantal character. Such level of theory goes beyond all previous reports (e.g. see Bryantsev and co-workers [16] and Mourad and co-workers [20]). CASSCF has been very recently exploited by Zaichenko [24] and co-workers to study the dissociation sequence $XO_2 \rightarrow X^+ + O_2^- \rightarrow X + O_2$ (with X=H, Li, Na, K) on both the triplet and singlet PES, to model a unimolecular superoxides homolytic bond cleavage. Zaichenko and co-workers demonstrate that CASSCF effectively allows to correctly model the electronic structure of O_2 both in triplet and singlet spin states, whereas the most common computational approaches, being based on a single reference paradigm, e.g. DFT or MP2, fail. We need to stress that a correct representation of O_2 electronic structure is mandatory for a

realistic description of the disproportionation reaction and to get rid of the inevitable computational bias at different levels of theory. To prove this point, in the supplementary information (note S1, tables S1 and S2) we report a survey of the computational determinations of the atomization energies for triplet/singlet dioxygen molecules and the corresponding vertical triplet singlet energy gap obtained with the most common single-reference approaches and the multi-reference ones. Only CASSCF/NEVPT2 yields a vertical triplet singlet energy gap in O_2 of decent accuracy.

Results and Discussion

The superoxide disproportionation reaction, in its fully ionic form, is:

$$O_2^- + O_2^- \rightarrow O_2^{2-} + O_2 \qquad \text{(R4)}$$

where a charge transfer process occurs through the migration of a single electron from one of the superoxide anions to the other. Inevitably, the double negatively charged pre-reaction complex ($O_2^-\cdots O_2^-$) has little or no chance to form due to Coulomb repulsion, and R4 requires a positively charged catalyst to occur. A well-known catalytic agent for reaction R4 is the proton which partially neutralizes the negative charge and makes the following reaction very efficient: [25,26]

$$HO_2 + O_2^- \rightarrow HO_2^- + O_2 \qquad \text{(R5)}$$

Another possible catalytic agent is the Li^+ ion which plays the same role of the proton:

$$LiO_2 + O_2^- \rightarrow LiO_2^- + O_2 \qquad \text{(R6)}$$

Both R5 and R6 can proceed on either a singlet or triplet PES. The typical qualitative reaction energy profile of R5 for one multiplicity is illustrated in Figure 1. The same profile holds for reaction R6.

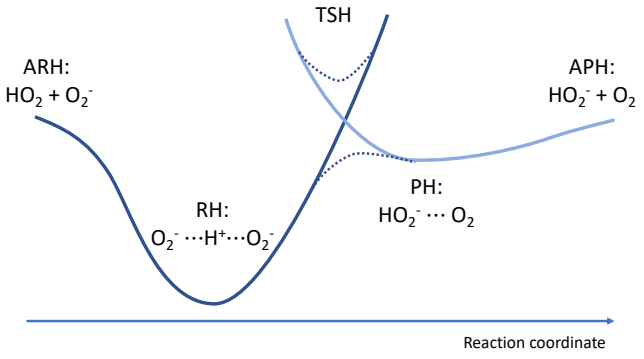

Figure 1. Purely schematic reaction profile for R5. Only one multiplicity is shown. The continuous lines are the two diabatic energies, the dotted ones are the two corresponding adiabatic ones. The naming convention adopted throughout the paper is also indicated.

In R5 there are, at least, 5 stationary points:

1. The isolated reactants (ARH) that correspond to HO_2 and O_2^- at infinite distance; the two partners are two doublets that can arrange themselves in either a triplet or a singlet total spin state with the same energy.
2. The pre-reaction complex (RH) which is a negatively charged $[O_2^-\cdot H^+\cdot O_2^-]$ adduct and is more stable than the separated reactants. This complex can be either in a singlet/triplet state.
3. The transition state (TSH) which is located near the crossing point of the two diabatic states.
4. The product complex (PH) which has the negative charge localized on the peroxide: $HO_2^-\cdots O_2$. The peroxide is a singlet specie, while the oxygen molecule can be in a singlet or triplet state.
5. The asymptotic products (APH) that correspond to a peroxide and an oxygen molecule infinitely separated: HO_2 and O_2.

The same scheme can be applied to the Li^+ catalyzed reaction, so that we have second set of structures, namely ARL, RL, TSL, PL and APL.

The reaction profile of Figure 1 follows quite straightforwardly a typical "Marcus" electronic transfer [27]. The transfer takes place at the point indicated by TSH where the reaction must pass through a crossing between two different diabatic electronic states (solid lines) of the same multiplicity (singlet or triplet). These crossing states, on the immediate left and right of TSH, differ only in the occupation of the orbitals. As a first approximation, it is possible to use the energy of the crossing point as an indicator of the energy of the transition state. In order to be more accurate, since the nuclear dynamics on two diabatic states is coupled, the corresponding, uncoupled adiabatic energies (dotted lines in Figure 1) must be computed near the crossing point. The exact location of the transition state for R5 and R6 depends, not only on the position of the crossing point, but also on the strength of the coupling and how much the adiabatic energies differ from the diabatic ones. Depending on the multiplicity of the initial reactant complex, the final oxygen molecule can be either in its (ground) triplet state or in its (first excited) singlet state. For this reason, in the rest of the present paper, we will present two sets of results for either singlet or triplet multiplicity.

The ground state, triplet minimum energy structures of R5 and R6 intermediates (RH and PH, RL and PL) are shown in Figure 2 (first row), along with their charge distribution (second row) and their spin densities (third row). The geometries of the corresponding singlet molecules are essentially identical or very similar.

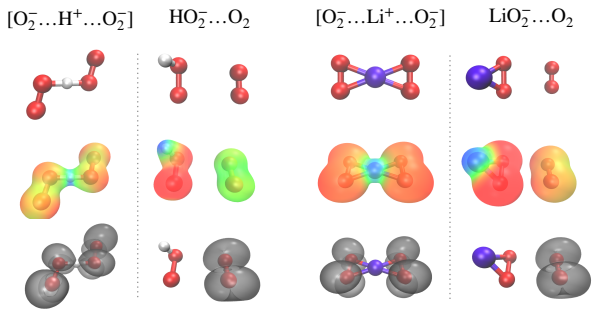

Figure 2. Top left: structures RH and PH. Top right: structures RL and PL. Below each structure we report the charge distribution as an electronic density iso-surface coloured by the value of the electric potential (red is negative, green is neutral, and blue is positive) and, in gray, the spin density of the triplet multiplicity.

No symmetry constraints have been applied in the structural relaxation, in order to ensure the identification of the minimum energy conformers for all species. The structural parameters and the respective electrostatic features of all species are reported in Tables S3 and S4 in the SI.

The pre-reaction complex (RH) of the H^+-catalyzed reaction is characterized by a structure where the two O_2^- molecules arrange themselves around the central proton in a "Z" geometry. The two H^+—O distances are essentially identical (1.2 Å, see Table S4). The negative charge in RH atoms as well as the unpaired spin density are delocalized over the oxygen atoms with a slight excess of them on the external ones (see Table S4, SI).

The outcome of the H^+ catalyzed reaction (PH) is constituted by two isolated species: a negatively charged peroxide ion and a neutral oxygen molecule. The O—O distance in the PH complex (1.22 Å) approximates to the O_2 isolated species. The unpaired spin density of the triplet state in PH is obviously delocalized over the neutral oxygen molecule, since the peroxide anion is a closed shell. By looking at the geometries of RH and PH in the top row of Figure 2, we see that the geometric rearrangement throughout the reaction involves the rotation of the OOH peroxide anion around its O—O axis.

Turning to the Li^+ case (right panel in Figure 2) we see that the pre-reaction complex (RL) is more symmetric than the H^+ one and has a planar shape where all 4 oxygen atoms are equivalently coordinated by the central Li^+ ion. The negative charge is symmetrically delocalized over the oxygen atoms (see Table S4) as well as the unpaired spin of the triplet state. In analogy to the proton mediated reaction, a rotation of the LiOO portion of RL around the O—O axis transforms it into the product complex PL. The latter, again, corresponds substantially to two separated molecules: the peroxide anion and the neutral oxygen molecule.

The thermodynamics of reactions R5 and R6 in vacuum is presented in Figure 3. The corresponding data are summarized in the Table 1 and 2 for R5 and R6 respectively. The thermodynamics of the same reactions in model solvents (DME and DMSO) are reported in the SI (Table S5 and Figure S1).

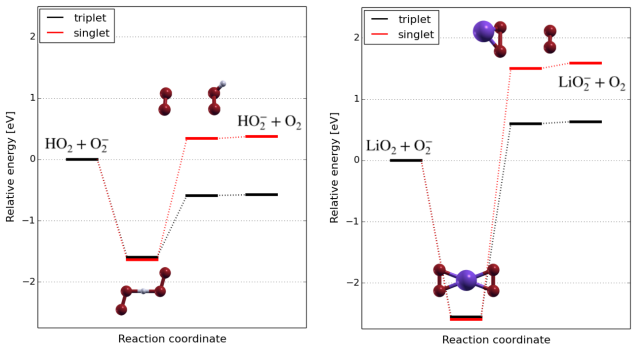

Figure 3. Thermodynamic of R5 (left) and of R6 (right) in vacuum. The pre-reaction complex and the product complex are indicated by explicit drawing of their structures. The asymptotic levels of separated reagents/products are indicated only by their stoichiometric formulas.

In tables 1 and 2, the last line (i.e. the energy of isolated products with respect to isolated reactants) is essentially the global energy change of the reaction, hence the 0 K temperature reaction enthalpy change $\Delta_r H$.

Both R5 and R6 reaction paths can be split in 3 steps:

(i) the formation of the pre-reaction complex (RH or RL) from isolated reagents;
(ii) its transformation into the product complex (PH or PL);
(iii) the dissociation to the isolated products.

Table 1. Energetics (in eV) of R5 on the triplet and singlet PES. The energy of APH with respect to ARH, reported in the last row, is the total enthalpy change of the reaction at zero temperature.

	Step	Reaction	Triplet PES	Singlet PES
(i)	ARH→RH	HO_2+ O_2^-→ O_2^-·H^+·O_2^-	–1.62	–1.62
(ii)	RH→PH	O_2^-·H^+·O_2^-→HO_2··O_2	+1.03	+1.96
(iii)	PH→APH	HO_2··O_2→HO_2^- + O_2	+0.01	+0.03
	ARH→APH	HO_2+ O_2^-→ HO_2^- + O_2	–0.58	+0.37

The triplet-singlet energy splitting is noticeable only for products, where we have the formation of a neutral oxygen molecule having a large energy difference between the two spin multiplicities. In fact, the triplet-singlet splitting is exactly zero for isolated reactants since the two superoxide anions are two doublets that can be indifferently arranged at infinite separation in either a singlet or a triplet state depending on the mutual orientation of their spin. The splitting is still negligible for the RH or the RL pre-reaction complexes, apparently violating WWSCRs. The violation originates from the fact that both pre-reaction complexes are held together by purely electrostatic interactions between the two superoxide anions and the positive charge of the catalyst (either H^+ or Li^+), and that covalency is very limited. Overall, both cations simply act as Coulomb screening agents which allow the two superoxide radicals to come into close contacts, thus overcoming their natural repulsion.

Table 2. Energetics (in eV) of R6 on the triplet and singlet PES. The energy of APL with respect to ARL reported in the last row is the total enthalpy change of the reaction at zero temperature.

	Step	Reaction	Triplet PES	Singlet PES
(i)	ARL→RL	LiO_2+ O_2^-→ O_2^-·Li^+·O_2^-	–2.58	–2.58
(ii)	RL→PL	O_2^-·Li^+·O_2^-→LiO_2··O_2	+3.18	+4.08
(iii)	PL→APL	LiO_2··O_2→LiO_2^- + O_2	+0.03	+0.09
	ARL→APL	LiO_2+ O_2^-→ LiO_2^- + O_2	+0.63	+1.59

In both multiplicities step (i), i.e. the formation of the pre-reaction complex (RH and RL), is an exoergic event ($\Delta E(i)<0$). The reagents adduct, in vacuo, is energetically more stable with respect to isolated reactants of about -1.6 eV and -2.6 eV for H^+ and Li^+ respectively. In model solvents, the concurrent solvation of both reactants and adducts (RH and RL) reduces $\Delta E(i)$ by roughly half.

In step (ii), i.e. the formation of product complexes (PH and PL) from the reagent complexes, the reaction follows different paths depending on the multiplicity. In particular, and as expected, we see that singlet oxygen molecules can be formed only as a

product on the excited state PES. Step (ii), is an endoergic process on both singlet and triplet PES. For the proton catalyzed reaction, the energy necessary to pass from RH to PH is 1 eV and 2 eV for the triplet and singlet PES respectively. When a model solvent is included, these numbers lower to few hundreds of meV for the triplet state and to slightly more than 1 eV for the singlet one (Table S5). For the Li^+ case, passing from RL to PL requires much more energy than for the proton case. In the gas phase the energy required in the triplet state is 3.2 eV and the one required in the singlet one is 4.1 eV. These energies are reduced to roughly half their values when in a model solvent.

The final step of R5 and R6 (step iii), i.e. the dissociation of the product complex, in vacuo, is weakly endoergic and essentially requires no energy. We have found that the energy of the product complexes $XO_2^-\cdots O_2$ is always very similar to its dissociated state XO_2^- + O_2 (X=Li or H). Although the ΔH of the final dissociation is very small, the entropic contribution ($T\Delta S$) of such step can be estimated to be around 0.3 eV (see section S6 in the SI) thus making its free energy difference negative.

We can summarize the overall thermodynamics of the cation-catalyzed disproportionation of two superoxides as follows:

- the reaction profile is qualitatively similar for both catalysts, H^+ and Li^+: a stable pre-reaction complex, a strongly exoergic evolution toward the products through an arguably "late" transition state and, finally, an almost isoergic dissociation of the product complex;
- for H^+ catalyzed reaction, the disproportionation path leading to triplet oxygen is globally exoergic of about -0.6 eV, in both the gas phase and in simulated solvent;
- for the H^+ catalyzed reaction, the formation of singlet oxygen is endoergic and requires 0.3-0.4 eV depending on the environment (vacuum or solvent);
- for the Li^+ catalyzed reaction the formation of triplet and singlet oxygen is a globally endoergic process of 0.6 eV and 1.6 eV respectively.
- In model solvents with a low (DME) or a large (DMSO) dielectric constant the thermodynamic landscape is very similar to the gas-phase, being the overall energy changes in the ARH→APH and ARL→APL reactions only slightly modified. We point out that, when computed in a solvent model, the last dissociation step P→AP becomes exoergic contrary to the gas-phase.

All these findings are in excellent agreement with the available experimental evidences for H^+ [25,26] and Li^+ [18-20] catalyzed superoxide disproportionation in aprotic media. In particular, the presently computed thermodynamics establishes the inaccessibility of a purely chemical pathway to $^1O_2$ release promoted by Li^+ under thermal condition. This finding confirms the evidences reported by Mourad and co-workers. [20] On the contrary, the presence of any trace of protons opens the door to singlet oxygen, thus feeding the formation of the most detrimental by-product in the Li-O_2 electrochemistry. Therefore, the control of the water content in solvents/salts, or that absorbed on high surface area porous positive electrodes, is of paramount importance to safely operate aLOBs as well as the minimization of any other side reactivity leading to proton release.

Turning to the kinetics of R5 and R6, the energy barriers of reaction RH→PH and RL→PL (steps (ii) in tables 1 and 2) have been evaluated by calculating a possible minimum energy path for both triplet and singlet multiplicities.

The results for the H^+ and Li^+ catalyzed reactions in the gas phase are summarized in the Figure 4. Since the thermodynamics turned out to be essentially the same in DMSO and DME (see SI and comment above), we have limited the analysis of the minimum energy paths only to the DME, a solvent commonly used in Li-O_2 batteries. The results for the reaction path in DME are presented in the SI in Figure S3.

In Figure 4, the pre-reaction complex RH and RL energy has been set to zero to facilitate the analysis of the kinetic barriers. However, it is important to recall that RH and RL are more stable than the isolated reagents ARH and ARL of about 1.6 and 2.6 eV, respectively. In the left panel, we see that the RH system evolves toward PH by internal torsion and by increasing the asymmetry of the O—H distances. For all the geometries before the first crossing point, the energy of the triplet and singlet states is essentially the same. Once the triplet PES reaches the first crossing point, one of the two O—H bonds break and the negative charge simultaneously migrates onto the resulting HO_2^- fragment leaving a triplet oxygen molecule (black triangles). If the system is in its singlet state, the energy needed to reach the second crossing point (red triangles) and for the break-up of the activated complex (with the formation of singlet oxygen) is much larger.

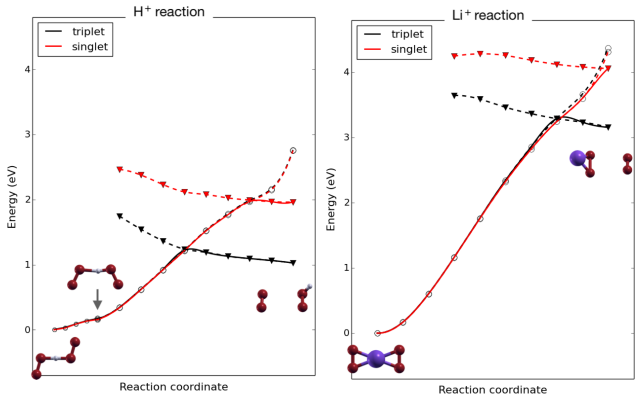

Figure 4. NEVPT2 energies along the minimum energy path of the ground state computed in the gas phase. The panel on the left is for H^+, that on the right is for Li^+. The dashed lines connect the 2-state CASSCF computations (roughly representing the diabatic states). The solid lines have been added as a guide for the eye to identify the lowest energy paths.

The energy location of the crossing points for both multiplicities clearly indicates the presence of very "late" transition states whose corresponding geometry is very similar to the products. In other words, the energetic separation of the singlet and triplet crossing points is very similar to the energetic separation of the final products. In the case of $O_2^-\cdot H^+\cdot O_2^-$, the triplet crossing energy is below (-0.39 eV) the initial reactants (ARH) energy, hence in agreement with the well-known established efficiency of the proton catalyzed disproportionation reaction.[25,26] The crossing point on the path to produce singlet oxygen is only slightly above (0.36 eV) the ARH energy. Overall, the energy barrier for $^1O_2$ release essentially coincides with the thermodynamic energy difference.

The situation for $O_2^-\cdot Li^+\cdot O_2^-$, is qualitatively similar, although now the crossing points for triplet and singlet oxygen formation occur at higher energies compared to the proton catalysis. Again, also for Li^+, the crossing point energies substantially coincide with the thermodynamic energy of final products.

Analogous calculations have been repeated using a DME solvent model and are presented in Figure S3. The main effect of

the dielectric presence is a decrease of the energy needed to reach the crossing points with respect to the gas-phase situation. This is expected because the crossing point is almost located at the geometry of the product complexes PH and PL which, being charged, are stabilized by the presence of the dielectric.

An overview of the energy of the diabatic crossing points and adiabatic activation energies is reported in Table 3 (and for the DME model solvent in Table S6)

Table 3. Energetic location of the diabatic crossing points (eV) for the overall ARH→APH and ARL→APL processes in vacuum. Estimate of the adiabatic kinetic energy barrier obtained by subtracting the adiabatic corrections to the diabatic crossing point (see text). Energies of the crossing points are reported respect to ARH/ARL. Energies of the barriers are reported with respect to ARH/ARL and RH/RL. The thermodynamic ΔE(ARH→PH) is also reported for comparison.

Spin	Diabatic crossing point	ΔE ARH→PH	Adiabatic energy barrier (respect to ARH/ARL)	Adiabatic energy barrier (respect to RH/RL)
HO_2+ O_2^-→ HO_2^- + O_2				
Triplet	-0.39	-0.59	none	~0.9
Singlet	+0.36	+0.34	~0.1	~1.7
LiO_2+ O_2^-→ LiO_2^- + O_2				
Triplet	+0.71	+0.60	~0.3	~2.9
Singlet	+1.50	+1.50	~1.0	~3.6

The diabatic crossing points can be discussed in comparison to the thermodynamic ΔE of the PH or PL complexes in respect to the isolated reagents (third column of table 3, same data of tables 1 and 2). Overall, we have two different situations: the crossing point for the singlet states essentially coincides with the energy of the products while is slightly higher than that for the triplet states. Therefore, if we take the crossing point as the likely structure of the transition state, we see that, at least for singlet states, the reaction of formation of PH/PL is substantially dominated by thermodynamics and, in this case, we do not expect any kinetic hindrance. For triplet states, on the other hand, we might see the appearance of small kinetic energy barrier due to the location of the crossing point being higher than APH/APL.

The diabatic energy crossings are only approximate indications of the kinetic hinderances between reagents and products: a more realistic estimate of the kinetic activation energies requires to evaluate the adiabatic energies (see Figure 1 for a graphical representation). In fact, in systems where the coupling between the two crossing states is large, the actual adiabatic states may differ considerably from the diabatic ones, thus leading to smaller activation energies.

In the SI (section S5) we show for all four diabatic crossings a set of calculations based on a 5-state CAS followed by a QD-NEVPT2 for Li^+ and H^+ catalysis. We have limited this calculation to the immediate surroundings of the crossing points and to the gas-phase. The crossing states interacts to a sufficient extent to lower the adiabatic energies with respect to diabatic ones. The extent of the adiabatic energy corrections is summarized in Table S6 in the SI. These corrections applied to the crossing point energies provides us with an estimate of the "true" barriers, as shown in the fourth/fifth column of Table 3. In all cases the resulting adiabatic barrier energies with respect to ARH/ARL are smaller than the energy of the PH/PL intermediates, hence we can conclude that for either H^+ or Li^+, for both the singlet and triplet PES the reaction is always dominated by thermodynamics and therefore we expect kinetic energy barriers to play a negligible role.

Conclusion

In summary, accurate multireference CASSCF/NEVPT2 calculations have been performed to simulate in vacuum and in model solvents the disproportionation reaction of superoxide anions catalyzed by H^+ and Li^+ ions. Both the singlet and triplet potential energy surfaces have been analyzed. The reaction pathways are qualitatively similar for both catalysts, H^+ and Li^+ in both spin multiplicities. The reaction mechanism involves three steps: (1) the formation of a stable pre-reaction complex; (2) a strongly exoergic evolution toward the products through a very "late" transition state and, finally, (3) an almost iso-energic dissociation of the product complex. By assuming the 1.0 eV qualitative energy threshold commonly adopted to identify active bimolecular reaction paths at room temperature,[28] our accurate thermodynamic data suggest the lack of any active purely chemical pathway to $^1O_2$ release promoted by Li^+, whereas the presence of any trace of protons discloses a facile thermodynamic channel to singlet oxygen release. Moreover, the analysis of the kinetic energy barriers suggests that all the modelled reactions are dominated by thermodynamics with activation energies almost negligible or absent.

Based on the present thermodynamic and kinetic evaluations, one may discuss the role played by the chemical superoxide disproportionation in aLOBs, where LiO_2 is produced as reaction intermediate either from the reduction of O_2 or the oxidation of Li_2O_2. Besides the ohmic drop, overpotentials applied to electrodes in an electrochemical cell allow to climb the energy barrier for the electron transfer and, this extra-work, is then transferred to the redox products, in our case LiO_2. Under the assumption of a direct energy transfer from the polarization overpotential to the kinetic internal energy of lithium superoxide, the application of large overpotentials can give LiO_2 enough kinetic energy to climb the activation energy for disproportionation at room temperature. Although this assumption is not fully correct, it approximates to a reasonable extent the overall energetics of an out-of-equilibrium polarized electrode with flowing current. Under this hypothesis, the LiO_2 disproportionation to triplet oxygen is kinetically barrierless if overpotentials larger than ~0.6 V are applied in respect to the thermodynamic $E°(O_2/Li_2O_2)$=3.0 V vs Li (i.e. below 2.4 V vs Li and above 3.6 V vs Li in ORR and OER, respectively).

On the other hand, barrierless singlet oxygen release via disproportionation requires the application of very large overpotentials of about ~1.5 V. This value, as well as the energy barrier for $^3O_2$ release, can be altered by the use of electrocatalysts[29] and therefore materials design for Li-O_2 electrochemistry must take into particular care the control of the singlet oxygen release paths.

Overall, one may conclude that the simple chemical disproportionation of LiO_2 is not directly involved in the $^1O_2$ release in aLOBs, operating in the narrow 2.5-3.5 V vs Li voltage range. In fact, LiO_2 molecules, produced as intermediate compound

either in the electrochemical reduction of O_2 or in the oxidation of Li_2O_2, need to overcome a 1.5 eV activation energy to release $^1O_2$, an energy barrier too high to be climbed at room temperature. However, the application of large overpotentials, beyond ±0.5 V, may reduce the net activation energy below 1.0 eV, therefore activating this reaction channel under the assumption of a direct energy transfer from the polarization overpotential to the kinetic internal energy of lithium superoxide. At small overpotentials, below ±0.5 V, the main source of singlet oxygen must be superoxide disproportionation catalyzed by H^+, standing the fact that protons act as extraordinary reaction boosters for both $^3O_2$ and $^1O_2$ releases. As an example, kinetically barrierless singlet oxygen release via H^+-mediated disproportionation requires the application of very small overpotentials of about ~0.3 V (i.e. below 2.7 V vs Li and above 3.3 V vs Li in ORR and OER, respectively). Therefore, we expect remarkable enhancements of the reversibility of the O_2/Li_2O_2 by the control of free protons originated by parasitic reactions, as an example by using H^+ traps.

Methods

All calculations have been performed using the Orca software version 4.1 [30] and using a model compound made by two superoxide anions O_2^- and one catalyst cation, H^+ or Li^+. Hence, the two molecular systems have the following stoichiometry: [H^+] [O_2^-] $_2$ and [Li^+] [O_2^-]$_2$.

The molecular orbitals at different nuclear geometries were optimized using a 2-state-averaged CASSCF (1 singlet + 1 triplet) with the ma-def2-TZVP basis set [31] within a [18, 12] active space. CASSCF wavefunctions were optimized using an equal weight for the singlet and triplet state. The corresponding correlated molecular energies were computed from the CASSCF orbitals with the multi-reference NEVPT2 method in its strongly contracted (SC) implementation. [32,33] The starting orbitals for the CASSCF calculations, have been generated using the natural orbitals coming from the (unrestricted) MP2 electronic density of the triplet state. In all computations, the resolution of identity (RI) approximation for the evaluation of two-electron integrals was employed, which allows remarkable time savings at the price of a negligible loss of accuracy. The [18, 12] active space was chosen to include all the *p*-type valence orbitals and electrons from the oxygens (12 orbitals, 18 electrons). The valence orbitals of the cations (*1s* of H and *2s* of Li), when included in the active space in a test calculation, turned out to be substantially inactive, with occupation numbers very close to zero; therefore, we excluded them in the final calculations, leading to a 18-in-12 active space.

The geometry optimizations of the pre- and post-reaction complexes, and of the isolated fragments have been done at the same CASSCF level as above, but the gradient of the energy has been computed only for the ground state by setting the weight of this state to 1 in the 2-state CASSCF calculation. We have not computed the zero point energies at the stationary points, therefore the latter is not included in our calculations. At the stationary points, additional optimizations have also been performed using the gradient of the excited state, but we detected only marginal differences in geometry. In order to calculate the global energy change of the reaction, the energy of the isolated fragments (peroxides, superoxides, superoxide anions, and neutral oxygen molecules) have been determined at the same level of theory and with the correct correspondence between the active orbitals in the isolated molecules and in the complexes, hence ensuring the size-consistency of the NEVPT2 energies.

Solvation effects have been accounted for using the conductor-like polarizable continuum model (C-PCM) [34], using the default implementation in the Orca code. The pre-set parameters for DMSO have been used and 1,2-dimethoxyethane (DME) has been modelled using the C-PCM default parameters, but changing the dielectric constant to ε=7.3; further increasing the dielectric constant has shown to produce very little changes on the energies.

Any attempt to locate the transition state with CASSCF is plagued by a number of problems: the CASSCF energies are very inaccurate (due to lack of correlation), and the presence of other low-lying additional singlet and triplet states (that are not relevant for the present study because they correlate with the wrong asymptotic states) can bring additional complications. For these reasons and, in order to quantify (at least qualitatively) the kinetic energy barriers to the reactions, we have calculated an approximate minimum energy path connecting the pre-reaction complexes to the post-reaction ones using the ground state triplet surface only. We have limited this calculation to the gas-phase and to the DME solvent model. Since the molecular rearrangement during the electron transfer reaction appears to be rather straightforward, and since the triplet state has a strong mono-determinantal character, a possible reaction path connecting reactants and products has been obtained by means of an unrestricted Kohn Sham calculation using the PBE functional in the triplet multiplicity. The geometries along the path have been obtained with the nudged elastic band (NEB) method to determine a reasonable minimum energy path connecting the stationary points at both ends of the reaction paths. At each of the PBE geometries the NEVPT2 energies have been computed using the multiconfigurational approach outlined above.

We have two sets of results: (i) those coming from a scan of the geometries along the path obtained starting from the right (reactants) and (ii) those obtained beginning the scan from the left (i.e. the products). Because of the severe constraint of our CASSCF to optimize exclusively one singlet and one triplet state, the two scans provide two different electronic states depending whether we are on the right or on the left of the crossing point. In this way we force the electronic states to maintain their occupation numbers and we have been able to trace, to a very good approximation, the *diabatic electronic PES's.* In order to understand our approach, we can look at Figure 1 in the main paper. The lowest-lying electronic state in each multiplicity (either triplet or singlet) has a different occupation pattern of the oxygen π orbitals depending if we are on the right or on the left of the crossing point. By forcing the CASSCF orbitals to optimize only one state for a given multiplicity, the resulting NEVPT2 energies are, in turn, forced to closely follow the *diabatic states* (solid lines in Figure 1) along the reaction path.

In order to compute also the *adiabatic electronic states* in the proximity of the crossing point (see again Figure 1) we have further characterized this region by performing a 5-state CASSCF[18, 12] calculation in either the singlet and triplet multiplicity followed by a quasi-degenerate QD-NEVPT2[35]. In this way we obtained fully *adiabatic* NEVPT2 energies and ensured that the lowest-lying NEVPT2 energies computed previously were not significantly influenced by the number of states used in the CAS step.

Acknowledgements

This work received financial support from “La Sapienza” (grant n. RM116154CA141A23). EB and SB gratefully acknowledge the computational support of CINECA (grants IscrC_AAAOX and IsC66_PSOxyR). SB thanks ENEA and MISE for the financial support through the PTR program 2019-2021.

Keywords: CASSCF/NEVPT2; disproportionation; LiO_2; $^1O_2$; batteries

[1] Y. C. Lu, B. M. Gallant, D. G. Kwabi, J. R. Harding, R. R. Mitchell, M. S. Whittingham, Y. Shao-Horn, *Energy and Environ. Sci.* **2013**, *6*, 750–768.

[2] L. Grande, E. Paillard, J. Hassoun, J.-B. Park, Y.-J. Lee, Y.-K. Sun, S. Passerini, B. Scrosati, *Adv. Mater.* **2015**, *27*, 784–800.

[3] J. Zhang, B. Sun, Y. Zhao, A. Tkacheva, Z. Liu, K. Yan, X. Guo, A. M. McDonagh, D. Shanmukaraj, C. Wang, T. Rojo, M. Armand, Z. Peng, G. Wang., *Nat. Comm.* **2019**, *10*, 1–10

[4] L. Johnson, C. Li, Z. Liu, Y. Chen, S. A. Freunberger, P. C. Ashok, B. B. Praveen, K. Dholakia, J. M. Tarascon, P. G. Bruce, *Nat. Chem.* **2014**, *6*, 1091–1099

[5] J. W. Choi, D. Aurbach, *Nat. Rev. Mater.* **2016**, *1*, 1–16.

[6] B. Scrosati, J. Garche, *J. Power Sources* **2010**, *195*, 2419–2430.

[7] D. Aurbach, B. D. McCloskey, L. F. Nazar, P. G. Bruce, *Nat. Energy* **2016**, *1*, 1–11.

[8] B. D. McCloskey, D. S. Bethune, R. M. Shelby, T. Mori, R. Scheffler, A. Speidel, M. Sherwood, A. C. Luntz, *J. Phys. Chem. Lett.* **2012**, *3*, 3043–3047.

[9] M. Carboni, A. G. Marrani, R. Spezia, S. Brutti, *J. Electrochem. Soc.* **2018**, *165*, 1–9.

[10] B. Adams, R. Black, Z. Williams, R. Fernandes, M. Cuisinier, E. J. Berg, P. Novak, G. K. Murphy, L. F. Nazar, *Adv. Energy Mater.* **2015**, *5*, 1–11.

[11] M. Carboni, A. G. Marrani, R. Spezia, S. Brutti, *Chem. Eur. J.* **2016**, *22*, 17188–17203.

[12] Y. Hong, C. Zhao, Y. Xiao, R. Xu, J. Xu, J. Huang, Q. Zhang, X. Yu, H. Li, *Batteries Supercaps* **2019**, *2*, 638–658.

[13] S. A. Freunberger, Y. Chen, N. E. Drewett, L. J. Hardwick, F. Bardé, P. G. Bruce, *Angew. Chem. Int. Ed.* **2011**, *50*, 8609–8613.

[14] Z. Peng, S. A. Freunberger, L. J. Hardwick, Y. Chen, V. Giordani, F. Bardé, P. Novák, D. Graham, J.-M. Tarascon, P. G. Bruce, *Angew. Chem. Int. Ed.* **2011**, *50*, 6351–6355.

[15] R. Black, J. H. Lee, B. Adams, C. A. Mims, L. F. Nazar, L. Black, R.; Lee, J. H.; Adams, B.; Mims A.; Nazar, *Angew. Chem. Int. Ed.* **2013**, *52*, 392–396.

[16] V. S. Bryantsev, M. Blanco, F. Faglioni, *J. Phys. Chem. A* **2010**, *114*, 8165–8169.

[17] U. Das, K. C. Lau, P. C. Redfern, L. A. Curtiss, *J. Phys. Chem. Let.* **2014**, *5*, 813–819.

[18] J. Wandt, P. Jakes, J. Granwehr, H. A. Gasteiger, R.-A. Eichel, *Angew. Chem.* **2016**, *128*, 7006–7009.

[19] N. Mahne, B. Schafzahl, C. Leypold, M. Leypold, S. Grumm, A. Leitgeb, G. A. Strohmeier, M. Wilkening, O. Fontaine, D. Kramer, C. Slugovc, S. M. Borisov, S. A. Freunberger, *Nat. Energy* **2017**, *2*, 17036.

[20] E. Mourad, Y. K. Petit, R. Spezia, A. Samojlov, F. F. Summa, C. Prehal, C. Leypold, N. Mahne, C. Slugovc, O. Fontaine, S. Brutti, S. A. Freunberger, *Energy Environ. Sci.* **2019**, *12*, 2559–2568.

[21] E. Wigner, E. E. Witmer, *Zeit. Phys.* **1928**, *51*, 859–886.

[22] K. E. Shuler, *J. Chem. Phys.* **1953**, *21*, 624–632.

[23] K. P. Huber, G. Herzberg, *Molecular Spectra and Molecular Structure*, Springer US, **1979**.

[24] A. Zaichenko, D. Schröder, J. Janek, D. Mollenhauer, *Chem. Eur. J.* **2020**, *26*, 2395–2404.

[25] C. P. Andrieux, P. Hapiot, J. michel Saveant, *J. Am. Chem. Soc.* **1987**, *109*, 3768–3775.

[26] Y. Che, M. Tsushima, F. Matsumoto, T. Okajima, K. Tokuda, T. Ohsaka, *J. Phys. Chem.* **1996**, *100*, 20134–20137.

[27] R. A. Marcus, *J. Electroanalytical Chem.* **1997**, *438*, 251–259.

[28] V. S. Bryantsev, V. Giordani, W. Walker, M. Blanco, S. Zecevic, K. Sasaki, J. Uddin, D. Addison, G. V. Chase, *J. Phys. Chem. A* **2011**, *115*, 12399-12409

[29] S.Cai, M. Zheng, X. Lin, M. Lei, R. Yuan, Q. Dong. *ACS Catalysis,* **2018**, *8*, 7983-7990

[30] F. Neese, The ORCA program system, *WIREs Comp. Mol. Sci.* **2012**, *2*, 73–78.

[31] J. Zheng, X. Xu, D. G. Truhlar, *Theor. Chem. Acc.* **2011**, *128*, 295–305.

[32] C. Angeli, R. Cimiraglia, S. Evangelisti, T. Leininger, J. P. Malrieu, *J. Chem. Phys*. **2001**, *114*, 10252.

[33] F. G. Kalatzis, I. N. Demetropoulos, *Mol. Phys*. **2007**, *105*, 2335–2343.

[34] V. Barone, M. Cossi, *J. Phys. Chem. A,* **1998**, *102*, 1995.

[35] C. Angeli, S. Borini, M. Cestari, R. Cimiraglia, *J. Chem. Phys.* **2004**, *121,* 4043–4049.